ACS OMEGA

http://pubs.acs.org/journal/acsodf

Article

Bismuth-Doped Nano Zerovalent Iron: A Novel Catalyst for Chloramphenicol Degradation and Hydrogen Production

Murtaza Sayed,* Aamir Khan, Sajid Rauf, Noor S. Shah,* Faiza Rehman, Abdullah A. Al-Kahtani, Javed Ali Khan,* Jibran Iqbal, Grzegorz Boczkaj, Ikhtiar Gul, and Maleeha Bushra

Cite This: *ACS Omega* 2020, 5, 30610−30624

Read Online

ACCESS | Metrics & More | Article Recommendations | Supporting Information

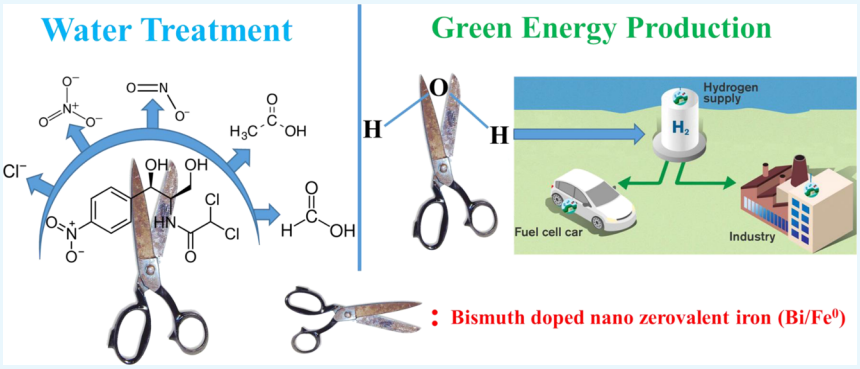

ABSTRACT: In this study, we showed that doping bismuth (Bi) at the surface of Fe^0 (Bi/Fe^0, bimetallic iron system)—synthesized by a simple borohydride reduction method—can considerably accelerate the reductive degradation of chloramphenicol (CHP). At a reaction time of 12 min, 62, 68, 74, 95, and 82% degradation of CHP was achieved with Fe^0, Bi/Fe^0-1 [1% (w/w) of Bi], Bi/Fe^0-3 [3% (w/w) of Bi], Bi/Fe^0-5 [5% (w/w) of Bi], and Bi/Fe^0-8 [8% (w/w) of Bi], respectively. Further improvements in the degradation efficiency of CHP were observed by combining the peroxymonosulfate (HSO_5^-) with Bi/Fe^0-5 (i.e., 81% by Bi/Fe^0-5 and 98% by the Bi/Fe^0-5/HSO_5^- system at 8 min of treatment). Interestingly, both Fe^0 and Bi/Fe^0-5 showed effective H_2 production under dark conditions that reached 544 and 712 μM by Fe^0 and Bi/Fe^0-5, respectively, in 70 mL of aqueous solution containing 0.07 g (i.e., at 1 g L^{-1} concentration) of the catalyst at ambient temperature.

1. INTRODUCTION

Environmental pollution and energy crises are the key issues that need urgent and global solutions. Among various environmental and water pollutants, the pharmaceuticals in the form of antibiotics pose a serious threat to human beings and other living species. Antibiotics are frequently used for inactivating and killing of micro-organisms. More than 250 different antibiotics/pharmaceuticals are extensively used for the treatment of humans, animal husbandry, and variety of plant diseases.[1,2] They, therefore, frequently enter into the fresh water bodies from pharmaceuticals industries, hospitals, husbandries, and homes. However, the presence of these antibiotics/pharmaceuticals in the fresh water bodies poses serious problems to terrestrial and aquatic life.[3] Among these widely detected antibiotics, chloramphenicol (CHP) is a broad spectrum antibiotic, used for deactivation of both Gram-positive and Gram-negative bacteria.[4] It has been reported that CHP is not fully digested in the human body and is defecated in urine and feces.[5] Because of its low molecular weight and high hydrophilicity, CHP cannot be completely eliminated from water by conventional methods such as coagulation, sedimentation, and filtration.[6,7] Efforts are going on continuously for the development of effective degradation methods of antibiotics. These methods mainly include advanced oxidation processes (AOPs) such as Fenton, photo-Fenton, and UV/H_2O_2, which mainly produce hydroxyl radicals ($^{\bullet}OH$) for the removal of these contaminants.[8−10] However, recently, sulfate radical ($SO_4^{\bullet-}$)-based AOPs have gained researcher's interest for the degradation of organic contaminants because of their higher removal efficiency. $SO_4^{\bullet-}$, having a redox potential of 2.5 V, is a strong and selective oxidant. Generally, peroxymonosulfate (PMS, HSO_5^-) and persulfate ($S_2O_8^{2-}$) are used as oxidants for the production of $SO_4^{\bullet-}$. PMS could produce both $^{\bullet}OH$ and $SO_4^{\bullet-}$ on activation. PMS can be activated by UV, heat, and transition metals.[11−14]

Received: September 17, 2020
Accepted: November 3, 2020
Published: November 19, 2020

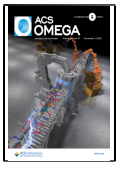

As far as the energy crisis is concerned, the green energy production in the form of H_2 from water splitting could provide a possible solution to this problem. H_2 is an ideal, clean and renewable energy source with outstanding advantages of high energy storage densities and environment-friendly (CO_2-free) reaction products. Different methods such as water gas shift ($CO + H_2O \leftrightarrow CO_2 + H_2$) and biogas dry reforming reactions through Pt/Ni-supported semiconductor catalysts have been applied for hydrogen production.[15,16] However, the replacement of the precious noble metal-based catalysts by the abundantly available cheap iron for economic production of H_2 is the need of the day.

Recently, nano zerovalent metals have emerged as inexpensive and effective activators for the activation of HSO_5^-.[17−19] In this regard, nano zerovalent iron (Fe^0) has gained considerable attraction because of its high reactivity for PMS activation and efficient reductive degradation of different contaminants such as heavy metals, pharmaceuticals, dyes, and pesticides.[20−22] Moreover, the application of Fe^0 for the production of H_2 has also been well documented.[23−25] The H_2 production from water decomposition by Fe^0 involves reduction of water and oxidation of Fe^0, that is, a redox reaction (reaction 1).[23]

$$Fe^0 + 2H_2O \rightarrow Fe^{2+} + 2OH^- + H_2 \rightarrow Fe(OH)_2 \downarrow + H_2 \quad (1)$$

Reaction 1 could also be considered as hydrogen evolution reaction (HER). The mechanism of HER is reported to be consisting of (i) formation of atomic H at the surface of catalyst, (ii) combination of H-atoms, and finally (iii) desorption of H_2 molecules.[23] The precipitate, $Fe(OH)_2$, is unstable under anaerobic conditions and may undergo a disproportionation reaction at temperatures >80 °C, that is, Schikorr reaction, leading to the formation of hydrogen and magnetite (Fe_3O_4) (reaction 2).[23,24,26]

$$3Fe(OH)_2 \rightarrow Fe_3O_4 + 2H_2O + H_2 \quad (2)$$

$Fe(OH)_2$ conversion to hydrogen and magnetite via reaction 2 is generally very slow or even not at all at room temperature. However, this reaction can be catalyzed by Fe^0.[24,27,28]

Thus, the overall redox reaction of water decomposition by Fe^0 can be summarized in the form of reaction 3.

$$3Fe^0 + 4H_2O \rightarrow Fe_3O_4 + 4H_2 \quad (3)$$

In summary, the overall stoichiometry of H_2 formation to Fe^0 could vary from 1:1 (reaction 1) to 4:3 (reaction 3). As the aforementioned HER could play an important role in clean fuel production through H_2 generation, recently, Fe^0 has received extensive attention of the researchers for its possible use for green energy production in addition to its use in water treatment processes for the effective removal of contaminants.

Furthermore, the magnetic characteristics of Fe^0 make it more attentional because of its easy separating and recycling ability from the aqueous solution under the external magnetic field.[29] However, because of its small size and surface effects, Fe^0 can easily be agglomerated via van der Waals and magnetically attractive forces, leading to the formation of bigger particles with significant loss in their reactivity.[29] In order to overcome this problem, many attempts have been made, for example, doping of Fe^0 with a second metal such as Pd, Au, Ag, Pt, Bi, and Cu.[30,31]

In the present study, we paid attention to synthesize bismuth-doped Fe^0 (Bi/Fe^0) as a novel and effective catalyst for the degradation of CHP from water as well as H_2 production from reductive decomposition of water. Bismuth (Bi) was selected as a dopant on account of its exceptional properties such as highly anisotropic Fermi surface, small effective mass, low carrier density, and long carrier mean free path.[30] Therefore, it is anticipated that the synthesized Bi/Fe^0 would effectively improve the reactivity of Fe^0 toward reductive degradation of CHP and activation of PMS. To date, HSO_5^- has been mainly activated by Fe^{2+}.[32,33] However, recently, the activation of HSO_5^- by Fe^0 has shown superior performance because of the maintainable formation of Fe^{2+}.[34]

2. EXPERIMENTAL SECTION

2.1. Materials. Iron(II) sulfate ($FeSO_4{\cdot}7H_2O$) was purchased from Sigma-Aldrich. CHP ($C_{11}H_{12}Cl_2N_2O_5$), oxone ($KHSO_5{\cdot}0.5KHSO_4{\cdot}0.5K_2SO_4$), ammonium chloride ($NH_4Cl$), methanol, and ethanol were provided by Sigma-Aldrich; sodiumborohydride ($NaBH_4$) and perchloric acid ($HClO_4$) 60% were purchased from Daejung, and bismuth nitrate ($BiNO_3$) was provided by Acros. All chemicals were used as received without further purification.

2.2. Synthesis of Fe^0 and Bi/Fe^0 Nanomaterials. The Fe^0 and Bi/Fe^0 nanomaterials were synthesized by a simple borohydride reduction method. For Fe^0, 1 g of $NaBH_4$ was dissolved in 40 mL of deionized (DI) water, and ferrous sulfate solution was prepared by dissolving 1 g of $FeSO_4$ in 25 mL of 25 vol % aqueous ethanol solution (18.75 mL DI water and 6.25 mL ethanol). The $NaBH_4$ solution was taken in a burette and that of $FeSO_4$ was transferred to the three-neck flask. The $NaBH_4$ solution was poured in a dropwise manner to the $FeSO_4$ solution under nitrogen gas purging with continuous stirring. The appearance of black particles indicated the formation of Fe^0. After completion of the reaction, the solution was stirred for 20 min. The Fe^0 particles were separated from the solution by centrifugation at 5000 rpm. The particles obtained were washed three times with ethanol to remove the impurities. The reduction of $FeSO_4$ by $NaBH_4$ occurs in accordance with reaction 4.[29]

$$Fe^{2+} + 2BH_4^- + 6H_2O \rightarrow Fe^0 \downarrow + 2B(OH)_3 + 7H_2\uparrow \quad (4)$$

For the synthesis of Bi/Fe^0 nanoparticles, the same process was followed except that the dopant precursor, bismuth nitrate ($BiNO_3$), was added in different proportions to $FeSO_4$ solution and stirred for 30 min for thorough mixing. The Bi/Fe^0 nanoparticles were then separated and washed three times with ethanol. The as-synthesized bare Fe^0 and Bi/Fe^0 nanoparticles were dried in a vacuum oven to avoid their oxidation. The samples were stored in ethanol prior to their characterization and testing. Different weight % of Bi, that is, 1, 3, 5, and 8 wt %, were doped at the surface of Fe^0 and were designated as Bi/Fe^0-1, Bi/Fe^0-3, Bi/Fe^0-5, and Bi/Fe^0-8, respectively.

2.3. Characterization. The morphologies of the as-synthesized Fe^0 and Bi/Fe^0 nanoparticles were investigated by scanning electron microscopy (SEM) (JEOL, JSM-5910) and transmission electron microscopy (TEM) (JEM-2011F, JEOL, Japan). Energy-dispersive X-ray (EDX) spectroscopy analysis was conducted by EDX (EX-2300BU, Jeol) for elemental analysis of the as-synthesized nanoparticles. To investigate the crystallinity of the as-synthesized nanoparticles,

https://dx.doi.org/10.1021/acsomega.0c04574
ACS Omega 2020, 5, 30610−30624

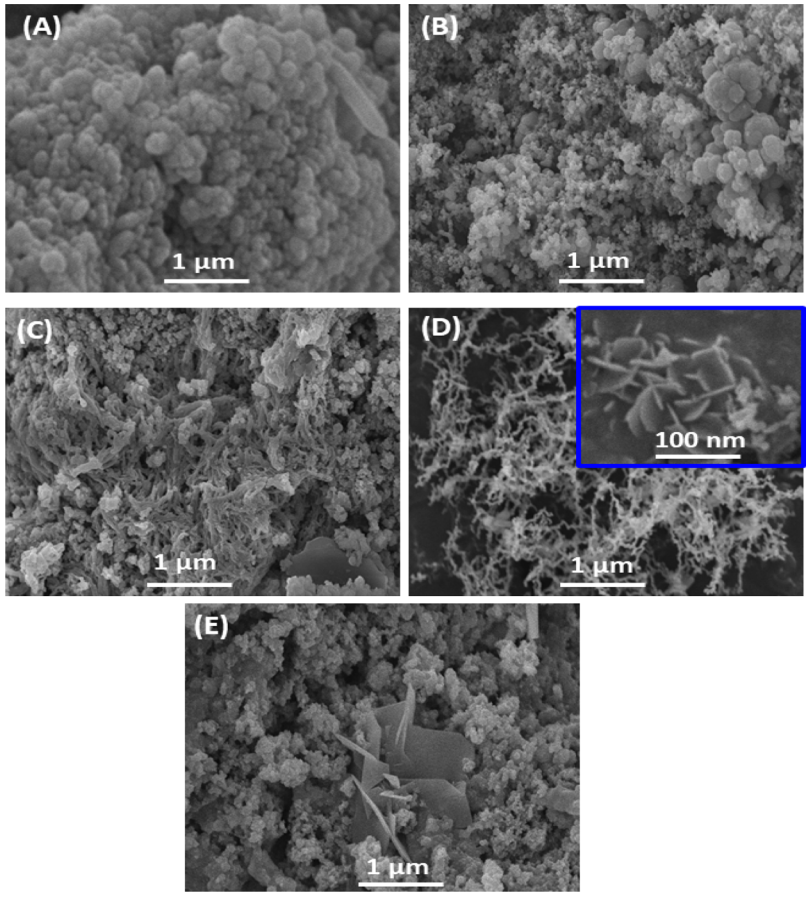

Figure 1. SEM images of Fe^0 (A), Bi/Fe^0-1 (B), Bi/Fe^0-3 (C), Bi/Fe^0-5 (D), and Bi/Fe^0-8 (E).

X-ray diffraction (XRD, PANalytical) analysis was performed using a Rigaku D/max-RB instrument with Cu Kα radiation (λ = 1.54 Å), operated at 45 kV and 100 mA. Thermogravimetric analysis (TGA) was conducted on a TG-DTA, PerkinElmer, system. The ultraviolet diffuse reflectance spectroscopy was performed on a PerkinElmer Lambda 35 UV−vis spectrometer (Shelton, CT, USA) using $BaSO_4$ as a reference. X-ray photoelectron spectroscopy (XPS) was conducted through PHI-5300, ESCA in which Al Kα was used as the source of X-ray excitation for studying the elemental composition and oxidation states of Fe and Bi. A quantachrome analyzer was used during the investigation of Brunauer−Emmett−Teller (BET) specific surface areas (S_{BET}), BJH pore size, and pore volume of the Fe^0 and Bi/Fe^0 nanoparticles.

2.4. Catalytic Activities of Fe^0 and Bi/Fe^0 Nanoparticles and the Analytical Procedure. The catalytic performance of Fe^0 and Bi/Fe^0 was investigated by the degradation of CHP in the presence and absence of HSO_5^-. The degradation experiments were performed in a 50 mL beaker containing 30 mL of reaction mixture. Unless stated otherwise, the initial concentration of CHP was 10 mg L^{-1}, the catalyst load was 1 g L^{-1}, pH = 6.8 and, when used, HSO_5^- was 1 mM. To ensure uniform mixing, the beaker was placed on a magnetic stirrer with constant stirring. The pH of the mixture was tuned with either perchloric acid ($HClO_4$) or sodium hydroxide (NaOH) when required. At predetermined time intervals, 0.5 mL of sample was taken for qualitative/quantitative analysis. The catalyst was filtered out before analyzing the samples. High-performance liquid chromatography (HPLC, Agilent 1200 series) was used for quantification of CHP. HPLC was equipped with a quaternary pump, a Eclipse XDB-C18 column (150 mm × 4.6 mm, particle size 5 μm), and a variable wavelength detector set at 270 nm. The mobile phase was pure methanol and water in the v/v ratio of 70:30 at a flow rate of 1 mL min^{-1} under isocratic mode. The injection volume was 20 μL, and the column temperature was 25 °C.

The cumulative concentrations of $SO_4^{\bullet-}$ and $^{\bullet}OH$ during the reaction process were quantified indirectly using hydroxybenzoic acid (HBA) and benzoic acid (BA) as chemical probes of $SO_4^{\bullet-}$[35] and $^{\bullet}OH$,[36] respectively. It has been reported that $SO_4^{\bullet-}$ on reaction with HBA results in the formation of hydroquinone which immediately transforms to stable 1,4-benzoquinone (BQ) in the presence of excess of PMS, while $^{\bullet}OH$ on reaction with BA gives *p*-HBA.[29] Each HBA and BA were used at 0.5 mM concentration (to ensure the complete conversion of $SO_4^{\bullet-}$ and $^{\bullet}OH$ into BQ and *p*-HBA, respectively) in the presence of 1 mM HSO_5^- and 1 g L^{-1} catalyst load, at pH = 6.8. At 2 min time intervals, 0.5 mL of samples were withdrawn, filtrated, and quenched with 100 μL EtOH. The generated BQ and *p*-HBA were detected and quantified by the same HPLC used for CHP quantification. The mobile phase was a mixture of acetonitrile and ultrapure water (50:50, v/v) at a flow rate of 1.0 mL min^{-1} for both BQ and *p*-HBA. The detection wavelength was set at 246 nm for BQ and 265 nm *p*-HBA.[37] The amount of generated BQ and *p*-HBA was thus used to calculate the concentration of $SO_4^{\bullet-}$ and $^{\bullet}OH$ in the reaction system. The concentrations of $SO_4^{\bullet-}$ and $^{\bullet}OH$ were calculated according to the stoichiometric ratio

https://dx.doi.org/10.1021/acsomega.0c04574
ACS Omega 2020, 5, 30610−30624

of $SO_4^{\bullet-}$ and BQ (1:1) and $^{\bullet}OH$ and *p*-HBA (5.9:1), respectively.[38]

The qualitative determination of the degradation products (DPs) of CHP was carried out by using liquid chromatography- mass spectrometry (LC/MS, Agilent Technologies), equipped with a C-18 column (150 × 4.6 mm, 1.7 μm particle size). The mass spectrometer was the Quattro Premier XE tandem quadrupole mass spectrometer having an electrospray ionization source. The mobile phase was composed of acetonitrile and methanol (1:3 v/v) with a flow rate of 1.5 mL min^{-1}. Electrospray interface was used at full scan mode from 50 to 500 *m*/*z*. The other mass constraints were established as follows: source temperature 110 °C, capillary voltage 2.2 kV, desolvation gas flow rate 635 L h^{-1}, and desolvation temperature 280 °C.

The recovery of the catalysts was done by using a magnet to separate catalysts from the aqueous media. The catalyst was then dried at 60 °C for 1 h and then applied for the next run.

2.5. Toxicological Assessment. To examine the toxicological (eco-toxicity) assessment of CHP and its DPs, Ecological Structure Activity Relationship (ECOSAR) build on computerized structure activity relationships was applied. According to the ECOSAR program, the acute and chronic toxicities of CHP and its DPs were estimated toward fish, daphnia, and green algae.[1] The acute toxicities (related to the adverse effects of a substance that result either from a single exposure or from multiple exposures in a short period of time) were expressed in terms of LC_{50} and EC_{50}, while chronic toxicities (defined as the adverse effects that result from long-term exposure) were measured from ChV values. LC_{50} can be defined as the concentration of pollutant that can demise 50% of daphnia and fish when applied for 48 and 96 h, respectively, whereas EC_{50} is the concentration of toxin liable for 50% inhibition of green algae growth when interacted for 96 h.[1]

2.6. Hydrogen Evolution Experiments. The H_2 production experiments were performed in a 100 mL Pyrex reaction cell containing 70 mL of DI water. In a typical H_2-production experiment, the Fe^0 and Bi/Fe^0-5 powders, at the desired concentrations, were added to the reaction cell at ambient temperature. Of note, DI water was purged with pure nitrogen gas for 45 min to remove the dissolved oxygen before the addition of Fe^0 or Bi/Fe^0-5 powders. During the experiment, the catalyst/DI water suspension was stirred at 300 rpm on a magnetic stirrer. The hydrogen gas was detected by gas chromatography (Agilent 7890 A) equipped with a 5 Å molecular sieve column and a thermal conductivity detector employing nitrogen as a carrier gas.

3. RESULTS AND DISCUSSION

3.1. Morphological, Structural, and Optical Characteristics of Fe^0 and Bi/Fe^0 Nanoparticles. Figure 1 represents the morphological characteristics of the as-synthesized Fe^0 and Bi/Fe^0 samples. It can be noticed that the as-synthesized Fe^0 particles are spherical in shape and are agglomerated most probably because of their magnetic nature (Figure 1A). However, the extent of agglomeration is decreased with increase in Bi content in Bi/Fe^0 nanoparticles along with reduction in particle size and the appearance of a cage type morphology (Figure 1B,C). Figure 1D shows a ring-shaped structure consisting of well-dispersed nanoplates (Figure 1D inset). Interestingly, when the Bi content was further increased to 8 wt % (Bi/Fe^0-8), the agglomeration again started to develop.

To get more details and in-depth morphological and structural information of the as-synthesized nanoparticles, (high resolution) TEM [(HR)-TEM] analysis was performed. TEM analysis shows that Bi/Fe^0-5 particles have a worm/vertical plate-like structure (Figure 2A). Furthermore, the

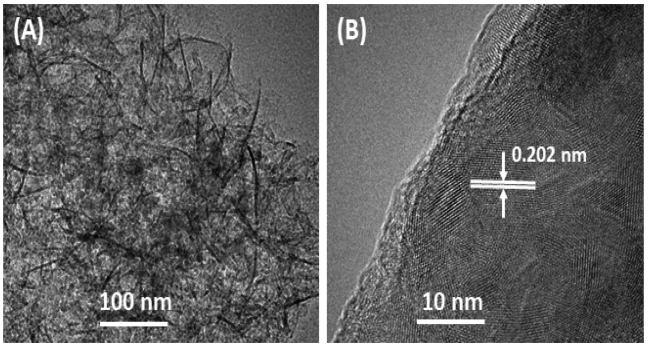

Figure 2. TEM image of the as-synthesized Bi/Fe^0-5 samples (A) and the corresponding HRTEM image (B).

particles are dense in distribution, and the dark color spots indicate the superposition of the crystal. This phenomenon anticipates that there would be a strong contact among particles and consequently would be able to show good adsorption. HR-TEM analysis showed that the interplanar space between two consecutive fringes was about 0.202 nm, which corresponds to the (110) plane of Fe^0 (Figure 2B).[39] Furthermore, the HR-TEM result indicates that the as-synthesized Bi/Fe^0-5 has a good single-crystal structure. The existence of a considerable amount of Fe^0 along with the calculated amount of Bi in the Bi/Fe^0-5 sample is well confirmed by EDX analysis (Figure S1). However, a small amount of carbon is also observed in EDX which could be coming from the glassware used for the sample preparation. The peak for sodium (Na) arises due to the use of sodium borohydride as the reducing agent in the synthesis process.

Figure 3 depicts the XRD patterns of the as-synthesized Fe^0 and Bi/Fe^0 samples. In all the patterns, a prominent peak at 2θ = 44.9° appears which corresponds to (110) facets of iron (Fe) having a cubic crystal system (JCPDS = 06-0696).

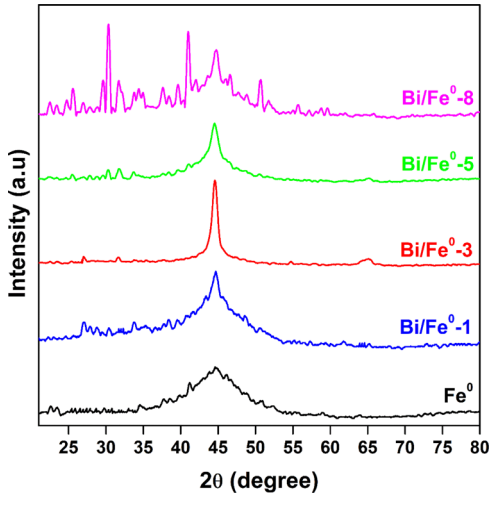

Figure 3. XRD spectra of the as-synthesized Fe^0, Bi/Fe^0-1, Bi/Fe^0-3, Bi/Fe^0-5, and Bi/Fe^0-8.

https://dx.doi.org/10.1021/acsomega.0c04574
ACS Omega 2020, 5, 30610−30624

Furthermore, it can be seen that while moving from Fe^0 to Bi/Fe^0-1 and then to Bi/Fe^0-3, the peak of Fe^0 becomes more pronounced, which slightly decreases for Bi/Fe^0-5, suggesting that Bi doping increases the crystallinity of Fe^0. However, for the Bi/Fe^0-8 sample, the satellite peaks in the 2θ range of 25−40° were observed, which are ascribed to the formation of oxides on the surface of the Fe^0.[40] Moreover, for the Bi/Fe^0-8 sample, the peaks at 2θ = 43.2, 53.32 and 57.36° correspond to magnetite (Fe_3O_4) (JCPDS = 01-1111) suggesting that excessive loading of Bi has oxidized Fe^0. The structural properties of the Fe^0 and Bi/Fe^0 samples are summarized in Table 1. It can be seen that the BET surface areas (S_{BET}) of the

Table 1. Physiochemical Characteristics of the As-Synthesized Fe^0, Bi/Fe^0-1, Bi/Fe^0-3, Bi/Fe^0-5, and Bi/Fe^0-8 Samples

samples	S_{BET} ($m^2\ g^{-1}$)	pore volume ($cm^3 g^{-1}$)	pore size (nm)[a]	porosity (%)[b]	particle size (nm)[c]	crystal size (nm)[d]
Fe^0	46.53	0.007	2.90	4..45	16.38	1.76
Bi/Fe^0-1	58.02	0.021	2.45	12.28	13.14	1.72
Bi/Fe^0-3	70.22	0.035	2.80	18.91	10.85	2.02
Bi/Fe^0-5	112.31	0.051	3.15	25.37	6.78	1.45
Bi/Fe^0-8	46.69	0.023	2.94	13.29	16.32	1.53

[a]Calculated from the pore radius of the adsorption isotherm. [b]Porosity (%) = pore volume ($cm^3\ g^{-1}$)/[pore volume ($cm^3\ g^{-1}$) + solid catalyst volume without pore ($cm^3\ g^{-1}$)] × 100. [c]Calculated from BET, using $D = 6000/(\rho \times S_{BET})$, where ρ = 7.87 g cm^{-3} of iron (Fe) density. [d]Measured from XRD data by applying Scherrer's equation; $D = 0.89\ \lambda/(B \times \cos\theta)$, where λ = 0.154 nm and B = full width at half-maximum (FWHM).

Fe^0, Bi/Fe^0-1, Bi/Fe^0-3, Bi/Fe^0-5, and Bi/Fe^0-8 samples correspond to 46.53, 58.02, 70.22, 112.31, and 46.69 $m^2\ g^{-1}$, respectively. The results showed that while going from Fe^0 to Bi/Fe^0-5, the S_{BET} increases from 46.53 to 112.31 $m^2\ g^{-1}$, indicating that Bi doping up to the optimum level inhibits the crystal growth of Fe^0.[1] However, the S_{BET} decreases to 46.69 $m^2\ g^{-1}$ for the Bi/Fe^0-8 sample possibly because of the agglomeration of Fe^0 particles at higher concentration of Bi. The same is also evidenced from their corresponding particle size (Table 1). The crystal sizes of the as-synthesized Fe^0, Bi/Fe^0-1, Bi/Fe^0-3, Bi/Fe^0-5, and Bi/Fe^0-8 samples were measured by a well-known Scherrer's equation[41] and found to be in the decreasing order of Bi/Fe^0-3 (2.02 nm) > Fe^0 (1.76 nm) > Bi/Fe^0-1 (1.72 nm) > Bi/Fe^0-8 (1.53 nm) > Bi/Fe^0-5 (1.45 nm) (Table 1). The porosity of the as-synthesized Fe^0, Bi/Fe^0-1, Bi/Fe^0-3, Bi/Fe^0-5, and Bi/Fe^0-8 samples corresponds to 4.45, 12.28, 18.91, 25.37, and 13.29%, respectively (Table 1). The high porosity and also surface area of Bi/Fe^0-5 make it favorable for strong adsorption of CHP on its surface, and thus, it is anticipated that the catalytic properties of Bi/Fe^0-5 would be excellent.

The XPS spectrum was recorded for better understanding the surface chemistry of the as-synthesized Bi/Fe^0-5 material (Figure 4). Figure 4A shows that the dominant species were Fe, O, Bi, and C on the surface of Bi/Fe^0-5 particles. The presence of Na (sodium) might be from $NaBH_4$ which was used for the reduction process in the synthesis of Bi/Fe^0-5. The position of C 1s peak at 284.5 eV is designated to the remaining carbon from the sample and adventitious hydrocarbon from the XPS instrument.[1] Figure 4B depicts the high-resolution Fe 2p XPS spectrum. The appearance of peak at 706.5 eV confirms the existence of Fe^0 (Fe $2p_{3/2}$).[42] Moreover, the existence of peak at 708.1 eV corresponds to the Fe^{3+} oxides (Figure 4B).[43] The presence of two peaks in the photoelectron spectrum of O 1s (at 530.3 eV and 531.9 eV) corresponds to the existence of hydroxyl bonded to metal (M − OH) and chemically or physically adsorbed H_2O on the surface of Bi/Fe^0-5, respectively (Figure 4C).[30] The high-resolution XPS spectrum of Bi 4f is separated into two large peaks at 159.3 and 164.1 eV corresponding to Bi $4f_{7/2}$ (Bi^{3+}) and Bi $4f_{5/2}$ (Bi^{3+}). Finally, the peaks at 162.6 and 158.1 eV are ascribed to Bi^0 (Figure 4D).

Figure 5 depicts the TGA of the Fe^0 and Bi/Fe^0-5 particles in the temperature range from 40 to 600 °C. In the case of Fe^0, it can be seen that there is gradual weight loss from 50 to 250 °C, which might be attributed to the evaporation of water and ethanol from the nanomaterial. However, at 430 °C, a dramatic increase in the weight of the Fe^0 nanomaterial was observed possibly because of the oxidation of Fe^0 (formation of oxides of iron). For the Bi/Fe^0-5 particles, initially there was rapid weight loss from 50 to 140 °C, which is attributed to the evaporation of water and ethanol. However, unlike Fe^0, no further prominent weight loss and gain was observed for Bi/Fe^0-5 which suggests that the thermal stability of the Bi/Fe^0-5 is increased due to Bi doping which prevents the formation of iron oxides and thus is in accordance with the XRD result.

3.2. Catalytic Degradation of CHP. The catalytic efficiencies of Fe^0 and Bi/Fe^0 nanoparticles were investigated for the degradation of CHP. Under the experimental conditions of $[CHP]_0$ = 10 mg L^{-1}, $[\text{catalyst load}]_0$ = 1 g L^{-1}, $[pH]_0$ = 6.8, and reaction time of 12 min, 62, 68, 74, 95, and 82% degradation of CHP was achieved by Fe^0, Bi/Fe^0-1, Bi/Fe^0-3, Bi/Fe^0-5, and Bi/Fe^0-8, respectively (Figure 6A). These results showed that the as-prepared nanomaterials follow the catalytic activity order in the sequence of Bi/Fe^0-5 > Bi/Fe^0-8 > Bi/Fe^0-3 > Bi/Fe^0-1 > Fe^0. The higher catalytic degradation efficiency of Bi/Fe^0-5 is due to its higher porosity and surface area which makes it more favorable for adsorption of CHP on its surface. Moreover, the formation of reactive oxygen species (ROS) on the surface of Bi/Fe^0-5 is much higher as compared to that of Fe^0, Bi/Fe^0-1, Bi/Fe^0-3, and Bi/Fe^0-8 nanomaterials, as depicted from their corresponding photoluminescence (PL) spectra (Figure S2), which leads to the higher removal of CHP by Bi/Fe^0-5 as compared to its counterparts.

Because Fe^0 is a strong reducing agent, it is expected that it could activate PMS (HSO_5^-) through an electron-transfer mechanism to generate reactive radicals in the form of hydroxyl and sulfate radicals ($^{\bullet}OH$ and $SO_4^{\bullet-}$). To test this hypothesis and further promote the catalytic activity of Bi/Fe^0-5 nanoparticles, the degradation of CHP was studied by the Bi/Fe^0-5/HSO_5^- system, and the results are depicted in Figure 6B. Interestingly, 98% CHP degradation was achieved by the Bi/Fe^0-5/HSO_5^- system as compared to 81% by Bi/Fe^0-5 under the reaction conditions of $[CHP]_0$ = 10 mg L^{-1}, $[HSO_5^-]_0$ = 1 mM, $[\text{catalyst load}]_0$ = 1 g L^{-1}, $[pH]_0$ = 6.8, and a reaction time of 8 min. Of note, only 8% CHP degradation was achieved by HSO_5^- alone under the same experimental conditions. It means that the sum of CHP degradation by Bi/Fe^0-5 and HSO_5^-, when used separately, is 89% (81% by Bi/Fe^0-5 + 8% by HSO_5^-) which is lower than that by the Bi/Fe^0-5/HSO_5^- system (98%). These results clearly indicated the synergism between HSO_5^- and Bi/Fe^0-5 which is possibly due

https://dx.doi.org/10.1021/acsomega.0c04574
ACS Omega 2020, 5, 30610−30624

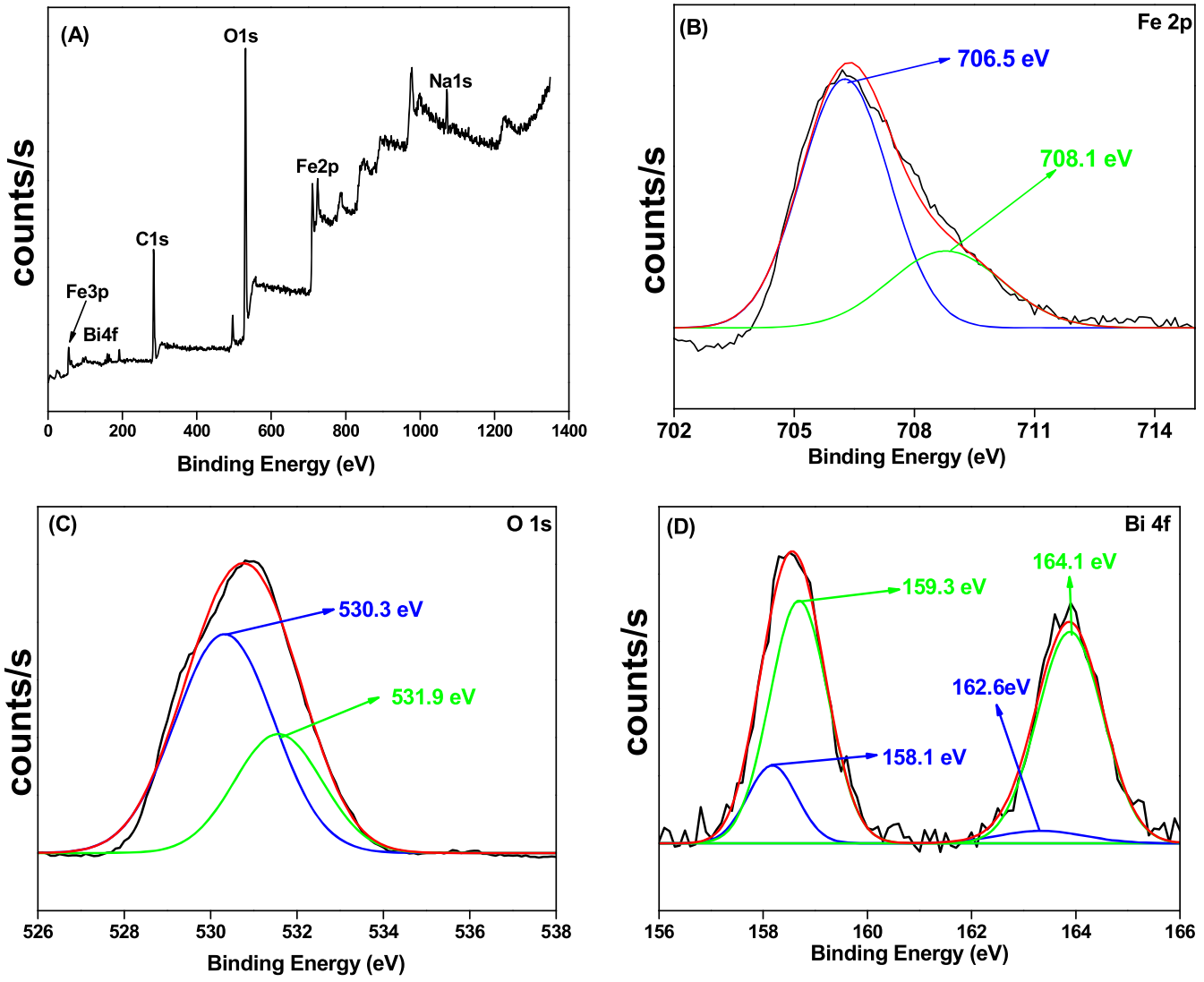

Figure 4. Full survey XPS spectra of Bi/Fe^0-5 (A), high-resolution Fe 2p high-resolution spectra (B), high-resolution O 1s high-resolution spectra (C), and high-resolution Bi 4f high-resolution peaks (D).

to the involvement of reactive radicals in the Bi/Fe^0-5/HSO_5^- system (reactions 5−12).[44,45]

$$Bi/Fe^0\text{-}5 + 2HSO_5^- \rightarrow Fe^{2+} + 2SO_4^{\bullet-} + 2OH^- \quad (5)$$

$$Bi/Fe^0\text{-}5 + 2HSO_5^- \rightarrow Fe^{2+} + 2SO_4^{2-} + 2^{\bullet}OH \quad (6)$$

$$Bi/Fe^0\text{-}5 + O_2 + 2H^+ \rightarrow Fe^{2+} + H_2O_2 \quad (7)$$

$$Fe^{2+} + HSO_5^- \rightarrow Fe^{3+} + SO_4^{\bullet-} + OH^- \quad (8)$$

$$Fe^{2+} + HSO_5^- \rightarrow Fe^{3+} + {}^{\bullet}OH + SO_4^{2-} \quad (9)$$

$$Fe^{2+} + H_2O_2 \rightarrow Fe^{3+} + {}^{\bullet}OH + OH^- \quad (10)$$

$$Fe^{2+} + HSO_5^- \rightarrow Fe^{2+} + SO_5^{\bullet-} + H^+ \quad (11)$$

$$Fe^{2+} + SO_4^{\bullet-} \rightarrow Fe^{3+} + SO_4^{2-} \quad (12)$$

The apparent rate constant (k_{app}) values are also depicted in Figure 6C and were found to be 0.0105, 0.2093, and 0.03253 min^{-1} for HSO_5^-, Bi/Fe^0-5, and Bi/Fe^0-5/HSO_5^-, respectively. These results reveal that the coupling of HSO_5^- with the Bi/Fe^0-5 is an effective way for accelerating the antibiotics degradation in the aqueous medium. To further investigate the reactivity of $^{\bullet}OH$ and $SO_4^{\bullet-}$ with CHP, second-order rate constants of $^{\bullet}OH$ and $SO_4^{\bullet-}$ with CHP ($k_{^{\bullet}OH/CHP}$ and $k_{SO_4^{\bullet-}/CHP}$) were measured using competition kinetics according to our previous report.[1] The *para*-chlorobenzoic acid (*p*-CBA, $k_{^{\bullet}OH/p\text{-}CBA} = 5.0 \times 10^9$ M^{-1} s^{-1}) and *meta*-toluic acid (*m*-TA, $k_{SO_4^{\bullet-}/m\text{-}TA} = 2.0 \times 10^9$ M^{-1} s^{-1}) were used as competitors for $^{\bullet}OH$ and $SO_4^{\bullet-}$, respectively.[46,47] The values of $k_{^{\bullet}OH/CHP}$ and $k_{SO_4^{\bullet-}/CHP}$ were measured to be 5.5×10^9 and 3.2×10^9 M^{-1} s^{-1}, respectively, which suggest comparable and higher reactivity of both $^{\bullet}OH$ and $SO_4^{\bullet-}$ with CHP.

3.3. Effect of pH on the Degradation of CHP by the Bi/Fe^0-5/HSO_5^- System. pH is one of the critical environmental parameters that could affect the removal efficiency of a water treatment technology. To investigate the effect of pH on the degradation of CHP by the Bi/Fe^0-5/HSO_5^- system, three different pH values (acidic, neutral, and alkaline) were studied, that is, 3.5, 6.8, and 10.5, respectively (Figure 7). It can be seen that as the solution pH increases from acidic to neutral and then to alkaline, the removal efficiency of CHP decreases. At a

https://dx.doi.org/10.1021/acsomega.0c04574
ACS Omega 2020, 5, 30610−30624

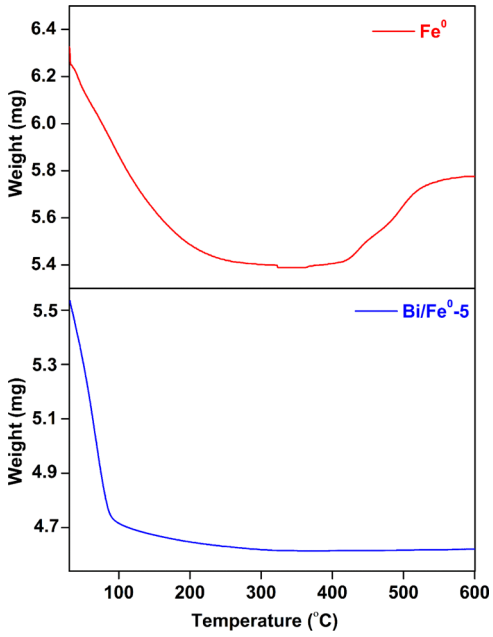

Figure 5. TGA curves of the as-synthesized Fe^0 and Bi/Fe^0-5 materials.

reaction time of 6 min, 93, 87, and 52% degradation of CHP was attained at pH 3.5, 6.8, and 10.5, respectively. The results indicate the strong influence of the initial solution pH on the catalytic degradation of CHP by the Bi/Fe^0-5/HSO_5^- system. This decrease in the catalytic degradation of CHP by the Bi/Fe^0-5/HSO_5^- system with the rise in pH from 3.5 to 10.5 could be due to the following three reasons. First, the pH of point of zero charge (pH_{PZC}) of Bi/Fe^0-5 was calculated to be 3.6 (Figure S3) which suggests that at pH > 3.6, the surface of Bi/Fe^0-5 is charged negatively. In other words, at pH > 3.6, the negative surface of Bi/Fe^0-5 repels the negative PMS anion. As a result, at higher pH values, less concentration of PMS would be catalyzed by Bi/Fe^0-5, which in turn led to the lower concentration of the reactive radicals. Second, the pK_a value of CHP is 9.5.[48] This means that at pH ≥ 10, CHP would exist in its anionic form in the solution, and consequently, very few CHP would be adsorbed on the surface of Bi/Fe^0-5 due to electrostatic repulsion. Third, the pH of solution affects the speciation of the PMS. The pK_{a1} and pK_{a2} of H_2SO_5 are less than 0 and 9.4, respectively. Therefore, at acid-neutral and basic conditions, the most dominant species of PMS are HSO_5^- and SO_5^{2-}, respectively.[48] Thus, at pH = 10.5, the predominant species of PMS is SO_5^{2-} which could scavenge both $^{\bullet}OH$ and $SO_4^{\bullet-}$ (reactions 13 and 14) and thereby reduce the degradation of CHP.[48] Of note, $SO_5^{\bullet-}$ is less reactive than $^{\bullet}OH$ and $SO_4^{\bullet-}$.

$$^{\bullet}OH + SO_5^{2-} \rightarrow SO_5^{\bullet-} + OH^- \quad (13)$$

$$SO_4^{\bullet-} + SO_5^{2-} \rightarrow SO_5^{\bullet-} + SO_4^{2-} \quad (14)$$

3.4. Identification of Reactive Species and Activation Mechanism of Bi/Fe^0-5/HSO_5^-. To investigate the participation of reactive species in the Bi/Fe^0-5/HSO_5^- system, quenching experiments were conducted by applying different radical scavengers. It has been well documented that in addition to $^{\bullet}OH$ and $SO_4^{\bullet-}$, $O_2^{\bullet-}$ and $^1O_2$ could form in the HSO_5^--activated system.[44] Ethanol (EtOH) is considered to be a strong scavenger of both $^{\bullet}OH$ (k = 1.2 to 2.8 × 10^9 M^{-1} s^{-1}) and $SO_4^{\bullet-}$ (k = 1.6 to 7.7 × 10^7 M^{-1} s^{-1}), whereas *tert*-butanol (TBA) is a well-known $^{\bullet}OH$ scavenger (k = 3.8 to 7.6 × 10^8 M^{-1} s^{-1}) but could not scavenge $SO_4^{\bullet-}$ efficiently because of its low rate constant with $SO_4^{\bullet-}$ (k = 4.0 to 9.1 × 10^5 M^{-1} s^{-1}). Furthermore, BQ and L-histidine (LH) were

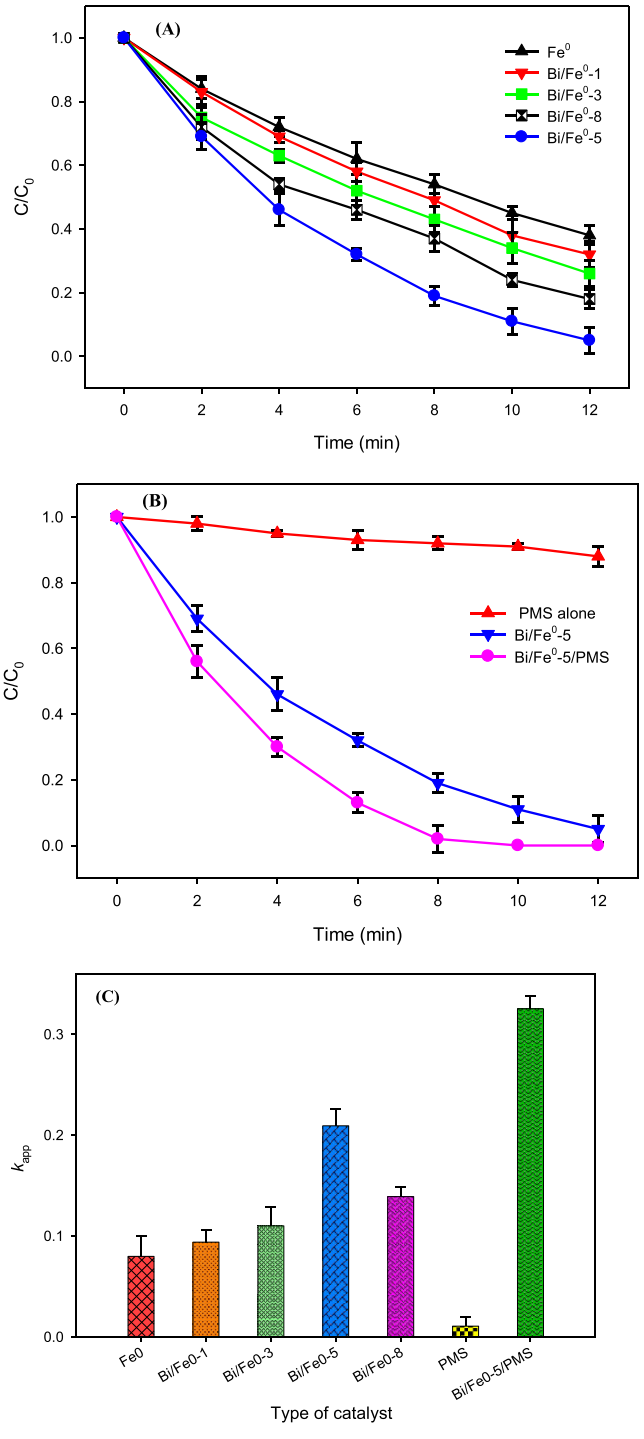

Figure 6. Catalytic degradation performance of the as-synthesized Fe^0, Bi/Fe^0-1, Bi/Fe^0-3, Bi/Fe^0-5, and Bi/Fe^0-8 materials (A); catalytic degradation of CHP by HSO_5^- alone, Bi/Fe^0-5 alone, and HSO_5^-/Bi/Fe^0-5 system (B) and comparison of the apparent rate constant (k_{app}) values of CHP degradation by Fe^0, Bi/Fe^0-1, Bi/Fe^0-3, Bi/Fe^0-5, Bi/Fe^0-8, HSO_5^- alone, and HSO_5^-/Bi/Fe^0-5 system (C). Experimental conditions: $[CHP]_0$ = 10 mg L^{-1}, $[pH]_0$ = 6.8, [catalyst load]$_0$ = 1.0 g L^{-1}, $[HSO_5^-]_0$ = 1.0 mM.

https://dx.doi.org/10.1021/acsomega.0c04574
ACS Omega 2020, 5, 30610−30624

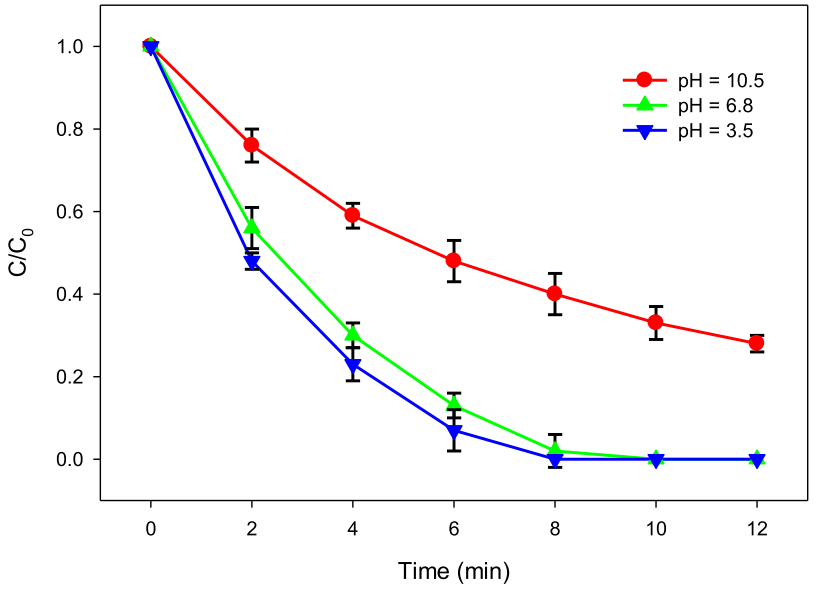

Figure 7. Effect of pH on the catalytic degradation of CHP by the HSO_5^-/Bi/Fe^0-5 system. Experimental conditions: $[CHP]_0$ = 10 mg L^{-1}, $[Bi/Fe^0\text{-}5]_0$ = 1.0 g L^{-1}, $[HSO_5^-]_0$ = 1.0 mM.

employed to inhibit the oxidation of CHP by $O_2^{\bullet-}$ and $^1O_2$, respectively, due to their high rate constants values ($k_{O_2^{\bullet-}/BQ}$ = 0.9 to 1.0 × 10^9 M^{-1} s^{-1} and $k'_{O_2/LH}$ = 5.0 × 10^7 M^{-1} s^{-1}).[29]

The results show that in the absence of a scavenger, 98% of CHP degradation was observed with k_{app} = 0.3253 min^{-1} at a reaction time of 8 min (Figure 8A). However, under the same experimental conditions, the % degradation of CHP reduced to 22 (k_{app} = 0.0307 min^{-1}), 63 (k_{app} = 0.1292 min^{-1}), 86 (k_{app} = 0.2439 min^{-1}), and 92% (k_{app} = 0.3063 min^{-1}) in the presence of EtOH, TBA, BQ, and LH (EtOH and TBA at 50 mM concentration, and BQ and LH at 1.0 mM concentration), respectively (Figure 8A). These results suggest that among $^{\bullet}OH$, $SO_4^{\bullet-}$, $O_2^{\bullet-}$, and $^1O_2$, the major species involved in the degradation of CHP by the Bi/Fe^0-5/HSO_5^- system is $SO_4^{\bullet-}$ followed by $^{\bullet}OH$ with some minor contribution from $O_2^{\bullet-}$ and $^1O_2$ as well.

To get more insights into the activation mechanism of the Bi/Fe^0-5/HSO_5^- system, the concentrations of $SO_4^{\bullet-}$ and $^{\bullet}OH$ during the reaction process were analyzed quantitatively. For this purpose, HBA and BA were chosen as representatives of $SO_4^{\bullet-}$[35] and $^{\bullet}OH$,[36] respectively. Figure 8B depicts the concentration of $SO_4^{\bullet-}$ and $^{\bullet}OH$ produced during the activation of HSO_5^- by Bi/Fe^0-5. As shown in Figure 8B, the cumulative concentration of $SO_4^{\bullet-}$ and $^{\bullet}OH$ steadily increased as the reaction proceed and reached 24.8 and 6.4 μM, respectively, at a reaction time of 10 min. Theoretically, 1000 μM (1 mM) of HSO_5^- could produce 1000 μM as the maximum cumulative concentration of $SO_4^{\bullet-}$ and $^{\bullet}OH$. This is because one HSO_5^- ion could produce one $SO_4^{\bullet-}$ or $^{\bullet}OH$ according to reactions 5−8. However, reaction 11 which is responsible for the cyclic generation of Fe^{2+} could reduce the formation of $SO_4^{\bullet-}$/$^{\bullet}OH$ as this reaction consumes one HSO_5^- ion without the production of $SO_4^{\bullet-}$/$^{\bullet}OH$. On the other hand, reactions 7 and 10 could lead to the formation of an additional $^{\bullet}OH$ without the consumption of the HSO_5^- ion. Another reaction which could result in the conversion of $SO_4^{\bullet-}$ to $^{\bullet}OH$ without changing the total concentration of $SO_4^{\bullet-}$ + $^{\bullet}OH$ may result in the decrease of $SO_4^{\bullet-}$ concentration and corresponding increase of $^{\bullet}OH$ concentration (reaction 15).[44]

$$SO_4^{\bullet-} + H_2O \rightarrow SO_4^{2-} + {}^{\bullet}OH + H^+ \quad (15)$$

It is noteworthy to be mentioned here that $SO_4^{\bullet-}$ and $^{\bullet}OH$ do not accumulate in the reaction mixture but rather continuously consumed by reacting with the target compounds. However, the products of the probe compounds, that is, BQ and *p*-HBA, may accumulate in the reaction mixture as long as their parent compounds, that is, HBA and BA, are available for their reaction with $SO_4^{\bullet-}$ and $^{\bullet}OH$. Therefore, the total concentrations of BQ and *p*-HBA were used to calculate the total concentration of $SO_4^{\bullet-}$ and $^{\bullet}OH$ produced in the reaction system from 0 to 10 min of reaction time in the present study. Moreover, the calculated concentration of BQ and *p*-HBA at different time intervals could be used to find out the $SO_4^{\bullet-}$ and $^{\bullet}OH$ concentration produced during the 2 min intervals (i.e., between 0 and 2, 2 and 4, 4 and 6 min, and so on) (see Table S1). It can be seen that the radical formation during the 2 min intervals is almost constant for both radicals, suggesting the steady-state formation of $SO_4^{\bullet-}$ and $^{\bullet}OH$ during the course of reaction. The steady-state formation of these radicals is due to the availability of their precursor (i.e., PMS) and its activator (Bi/Fe^0-5) in the reaction mixture up to the studied treatment time. The result of $SO_4^{\bullet-}$ and $^{\bullet}OH$ concentration is consistent with the radical scavenging results of higher contribution of $SO_4^{\bullet-}$.

On the basis of the above discussion, the detailed activation mechanism of HSO_5^- by Bi/Fe^0-5 is illustrated in Scheme 1. The as-synthesized Bi/Fe^0-5 through corrosion either by oxygen (O_2) or by HSO_5^- results in the formation of Fe^{2+} and Fe^{3+}. Afterward, Fe^{2+}/Fe^{3+} results in the formation of $^{\bullet}OH$ and $SO_4^{\bullet-}$.[44] These produced $^{\bullet}OH$ and $SO_4^{\bullet-}$ participate in the catalytic degradation of CHP; however, scavenging reactions may also occur if the concentration of these ROS ($^{\bullet}OH$ and $SO_4^{\bullet-}$) exceeds the optimum value. Furthermore, the in situ produced H_2O_2 also reacts with Fe^{2+} producing $^{\bullet}OH$. The other ROS such as $^1O_2$ and $O_2^{\bullet-}$ are also generated by the reaction of HSO_5^- with H_2O after a series of reactions.[44]

https://dx.doi.org/10.1021/acsomega.0c04574
ACS Omega 2020, 5, 30610−30624

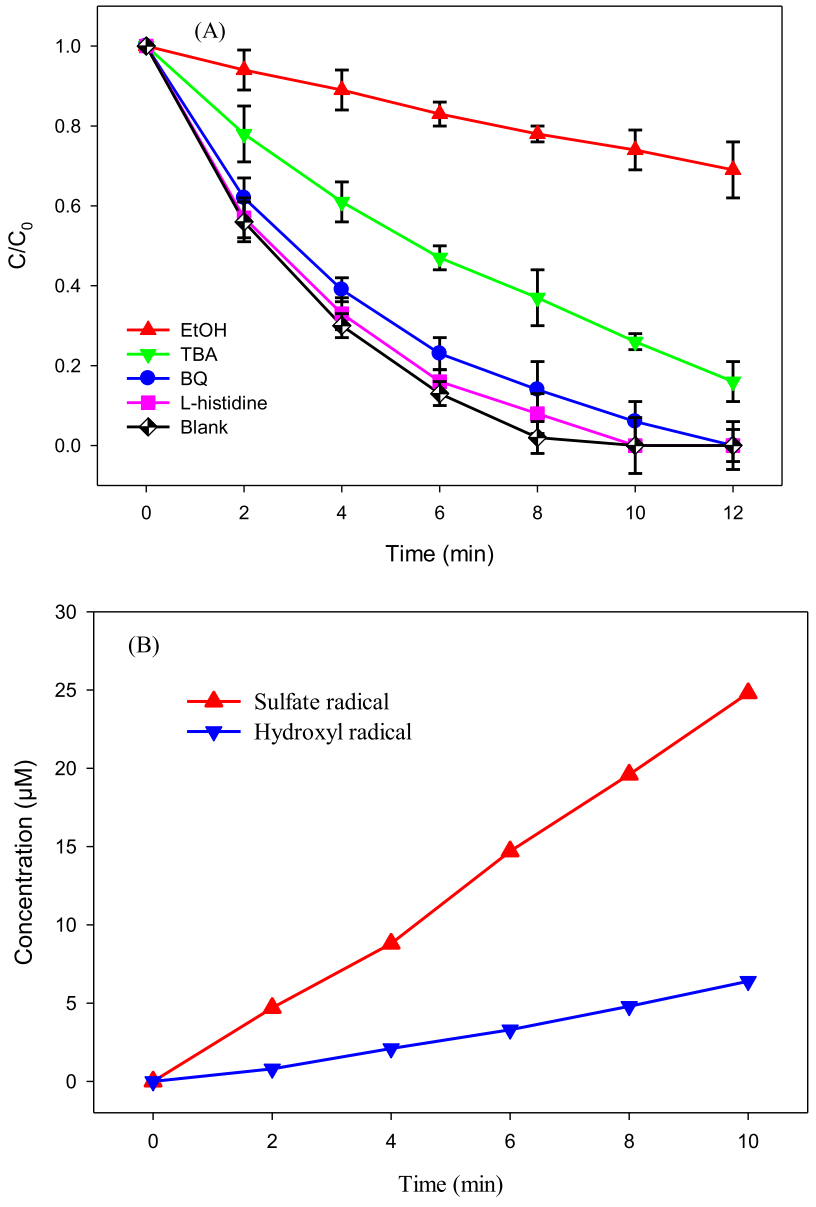

Figure 8. Effect of different scavengers (EtOH, TBA, BQ, and LH) on the catalytic degradation of CHP by the HSO_5^-/Bi/Fe^0-5 system (A) and formation of [$^\bullet$OH] and [$SO_4^{\bullet-}$] during HSO_5^-/Bi/Fe^0-5 system at different reaction times (B). Experimental conditions: $[CHP]_0$ = 10 mg L^{-1}, $[Bi/Fe^0\text{-}5]_0$ = 1.0 g L^{-1}, $[HSO_5^-]_0$ = 1.0 mM, $[pH]_0$ = 6.8, $[EtOH]_0$ = $[TBA]_0$ = 50 mM, and $[BQ]_0$ = $[LH]_0$ = 1.0 mM (A); $[Bi/Fe^0\text{-}5]_0$ = 1.0 g L^{-1}, $[HSO_5^-]_0$ = 1.0 mM, $[pH]_0$ = 6.8, $[HBA]_0$ = 0.5 mM (for $SO_4^{\bullet-}$ determination); $[BA]_0$ = 0.5 mM (for $^\bullet$OH determination) (B).

These generated reactive species ($^\bullet$OH, $SO_4^{\bullet-}$, $^1O_2$, and $O_2^{\bullet-}$) have sufficient ability to oxidize any target contaminants by a radical/nonradical way. Furthermore, various iron hydroxides such as $Fe(OH)_2$ and $Fe(OH)_3$ may also be generated during the reaction. These hydroxides could remove CHP and its DPs through adsorption.[49] It has been documented that these hydroxides are further transformed through dehydration and crystallization into Fe_2O_3, Fe_3O_4, and FeOOH, which have comparatively less adsorption capability,[44] although they could activate HSO_5^- to produce $SO_4^{\bullet-}$.[44]

3.5. Assessment of DPs and Their Ecotoxicity. An effective water treatment technology is the one which could reduce the overall toxicity of the treated water. Therefore, to find out the effectiveness of the Bi/Fe^0-5/HSO_5^- system for the treatment of antibiotics, in this CHP, the DPs of CHP and their ecotoxicities toward three aquatic organisms, that is, fish, daphnia, and green algae, were assessed. A total of nine DPs were identified. The details about these DPs are summarized in Table S2 (Supporting Information) along with their structure, chemical formula, and m/z values. A possible degradation pathway of CHP was proposed based the identified DPs (see Scheme 2). It can be seen that attack of $^\bullet$OH/$SO_4^{\bullet-}$ on CHP results in the formation of various hydroxylated DPs, in accordance with the previous study.[50] The first pathway (pathway-I) was initiated by the cleavage of the C−N bond with the loss of dichloroacetamide and thus result in the formation of DP2 with m/z = 195. DP2 is further dehydrated and gave rise to DP3 with m/z = 179. The second pathway (pathway-II) involves the elimination of the methanol group from the propylene glycol branch of CHP and gives rise to the formation of DP4 with m/z of 293, which further results in the formation of DP10 (dichloro-acetamide) with m/z = 128. Further attack of $^\bullet$OH/$SO_4^{\bullet-}$ on DP4 (pathway-IIB) oxidizes the lateral group and results in the substitution of $-NO_2$ with

https://dx.doi.org/10.1021/acsomega.0c04574
ACS Omega 2020, 5, 30610−30624

Scheme 1. Proposed Activation Mechanism of HSO_5^- by the As-Synthesized Bi/Fe^0-5

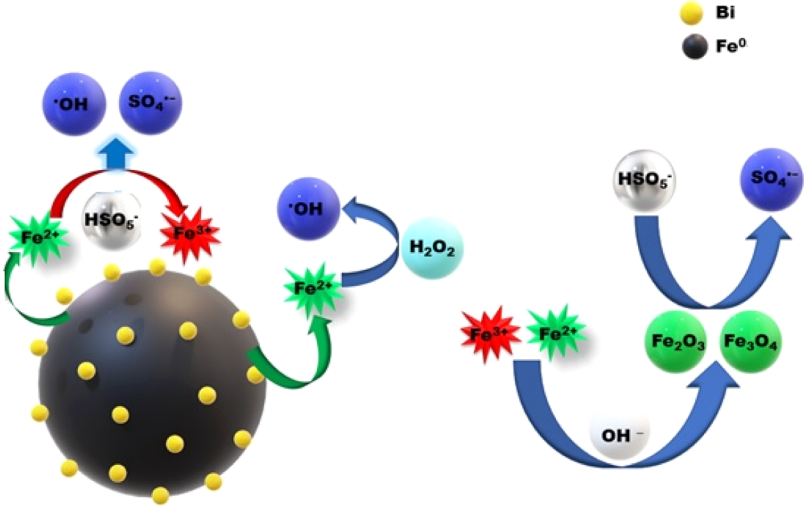

Scheme 2. Pathways for the Degradation of CHP by the Bi/Fe^0-5/HSO_5^- System

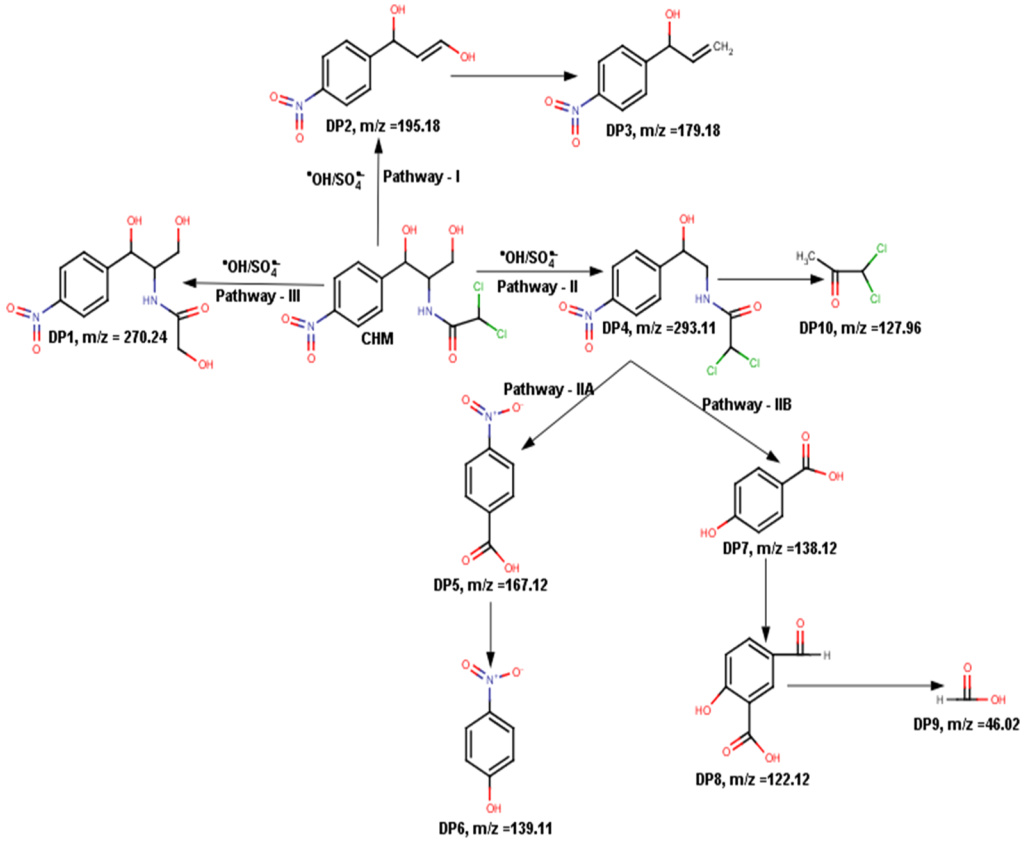

the OH group leading to the formation of DP7 (4-HBA) with m/z = 138. DP8 (4-hydroxy benzaldehyde) with m/z = 122 is formed due to the dehydroxylation of 4-HBA (DP7). The formation of DP9 (formic acid) with m/z = 46 suggests the effective oxidation of CHP into shorter chain acids. DP4 can also proceed further through degradation route II-A which involves hydroxylation followed by decarboxylation and results in the formation of DP5 (4-nitro benzoic acid) with m/z = 167, which further through decarboxylation gives DP6 (4-nitrophenol) having m/z = 139. The degradation pathway-III suggests the dechlorination of CHP by the attack of $^{\bullet}OH/SO_4^{\bullet-}$ and results in the formation of DP1 with m/z = 270.

The % removal of total organic carbon (TOC) was investigated for Bi/Fe^0-5 and Bi/Fe^0-5/HSO_5^- processes, and the results are shown in Figure S4. At a reaction time of 240 min, the % removal of TOC in the case of the Bi/Fe^0-5/HSO_5^- system was increased from 65 (Bi/Fe^0-5) to 92%, which could be due to the production of additional $SO_4^{\bullet-}$ in the case of the Bi/Fe^0-5/HSO_5^- process. Furthermore, it can be seen that in the case of the Bi/Fe^0-5/HSO_5^- system, after a reaction time of 120 min, there is a rapid increase in the %

https://dx.doi.org/10.1021/acsomega.0c04574
ACS Omega 2020, 5, 30610−30624

Table 2. Calculation of Ecotoxicity of CHP and Its DPs toward Different Aquatic Organisms in the Units of mg/L[a]

	acute toxicity			chronic toxicity		
compound	fish (LC_{50}) duration 96 h	daphnia (LC_{50}) duration 48 h	green algae (EC_{50}) duration 96 h	fish (ChV)	daphnia (ChV)	green algae (ChV)
CHP	883.0	643.0	185.0	62.0	81.5	70.2
DP1	2.04×10^4	1.31×10^4	2.01×10^3	1.01×10^3	1.09×10^3	492
DP2	405	298	90.5	29.3	39.1	35.5
DP3	107	82.7	31.8	8.83	12.7	14.7
DP4	910	660	185	63	82.2	69.1
DP5	2.60×10^3	1.43×10^3	949	245	129	233
DP6	21.9	9.11	1.92	2.15	0.98	3.99
DP7	491	162	42.3	45.7	15.9	77.7
DP8	17.3	17	9.19	3.61	0.16	3.20
DP9	6.13×10^3	2.77×10^3	807	458	144	127
DP10	55.8	80.3	1.07	29.2	85	1.06

[a]Acute toxicities based on the European Union criteria (described in Annex VI of Directive 67/548/EEC) as $LC_{50} > 100$ or $EC_{50} > 100$ (not harmful), $10 < LC_{50} < 100$ or $10 < EC_{50} < 100$ (harmful), $1 < LC_{50} < 10$ or $1 < EC_{50} < 10$ (toxic), and $LC_{50} < 1$ or $EC_{50} < 1$ (very toxic). While chronic toxicities assessed based on the Chinese hazard evaluation criteria for new chemical substances (HJ/T154-2004), that is, ChV > 10 (not harmful), 1 < ChV < 10 (harmful), 0.1 < ChV < 1 (toxic), and ChV < 0.1 (very toxic).

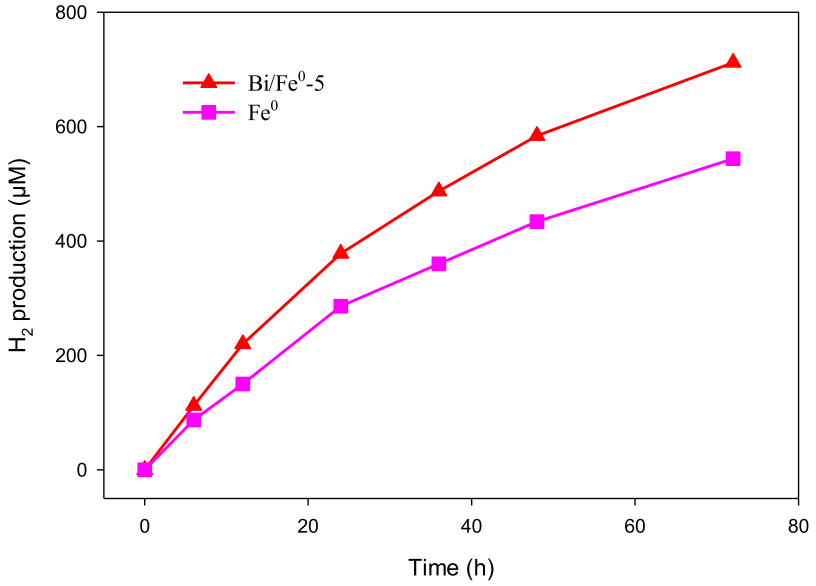

Figure 9. Hydrogen production from water decomposition by Fe^0 and Bi/Fe^0-5 nanoparticles. Experimental conditions: $[Fe^0]_0 = [Bi/Fe^0\text{-}5]_0 = 1.0$ g L^{-1}, $[pH]_0 = 6.8$, reaction solution = 70 mL (containing 0.07 g of catalyst).

removal of TOC from 36 to 58%; however, in the case of Bi/Fe^0-5 process, it was just increased from 28 to 33% (Figure S4). This indicates the mineralization of persistent DPs of CHP by the Bi/Fe^0-5/HSO_5^- system due to additional involvement of $SO_4^{\bullet-}$ along with $^{\bullet}OH$ in the mineralization of CHP. The higher % removal of TOC for CHP by the Bi/Fe^0-5/HSO_5^- system implies that this process can be successfully applied in batch-scale reactors for contaminated water treatments.

For the practical implementation of any treatment technique, it is necessary to investigate the cyclic catalytic performance. To study the cyclic catalytic performance of the as-synthesized Bi/Fe^0-5 material coupled with HSO_5^-, twelve (12) consecutive cyclic degradation runs were performed, and the results are shown in Figure S5. After each run, the catalyst was washed and dried and then reapplied without any additional regeneration treatment. It can be seen that till the 6th run, the catalytic degradation performance of the proposed Bi/Fe^0-5/HSO_5^- system was almost constant; however, afterwards, it slowly started to decrease from 93 to 85% at the 12th run (Figure S5). This decrease in the catalytic performance of Bi/Fe^0-5/HSO_5^- was probably due to the adsorption of DPs of CHP on the active sites of Bi/Fe^0-5, which prevents further adsorption and thus decreases the degradation of CHP over the surface of Bi/Fe^0-5. However, these adsorbed DPs can easily be desorbed by vacuum drying of the as-synthesized material at 80 °C. The successful stable catalytic performance of the Bi/Fe^0-5/HSO_5^- system till 6th runs further provides an evidence that the proposed treatment technique is not only efficient but also economical for the treatment of organic contaminants.

To further evaluate the practical applicability of the Bi/Fe^0-5/HSO_5^- system, the ecotoxicity of these detected DPs toward fish, daphnia, and green algae was assessed using the ECOSAR program. The toxicity results are presented in Table 2 and Figure 10. The results show that CHP and its DPs have varied levels of ecotoxicity toward different organisms, and most of the DPs have even higher toxicity than CHP. This opens a new window for environmental researcher to think about these DPs and to find new ways to effectively eliminate them. However,

https://dx.doi.org/10.1021/acsomega.0c04574
ACS Omega 2020, 5, 30610−30624

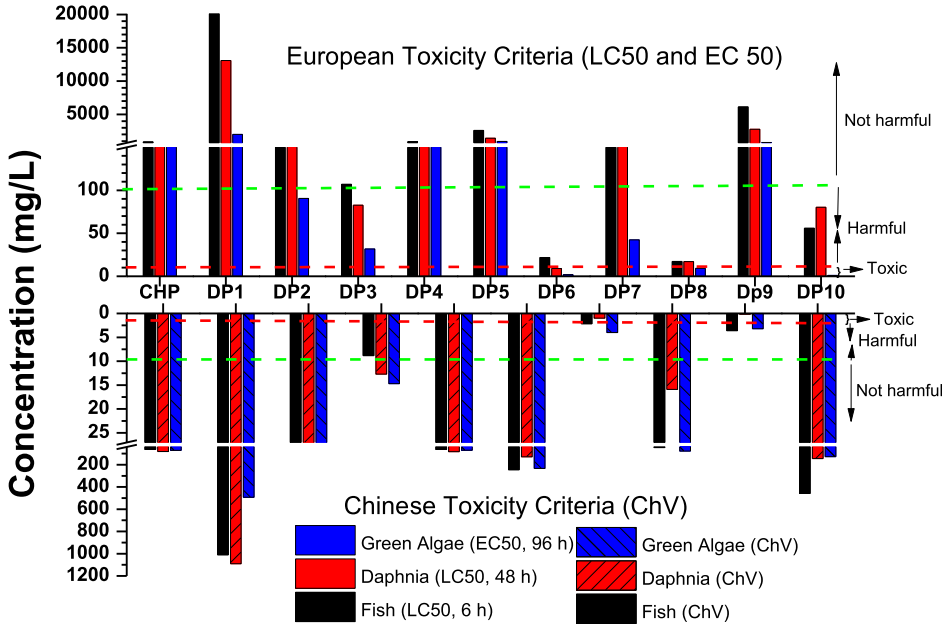

Figure 10. Calculation of ecotoxicity of CHP and its DPs toward different aquatic organisms in the units of mg/L. Acute toxicities based on the European Union criteria (described in Annex VI of Directive 67/548/EEC) as $LC_{50} > 100$ or $EC_{50} > 100$ (not harmful), $10 < LC_{50} < 100$ or $10 < EC_{50} < 100$ (harmful), $1 < LC_{50} < 10$ or $1 < EC_{50} < 10$ (toxic), and $LC_{50} < 1$ or $EC_{50} < 1$ (very toxic), while chronic toxicities assessed based on the Chinese hazard evaluation criteria for new chemical substances (HJ/T154-2004), that is, ChV > 10 (not harmful), 1 < ChV < 10 (harmful), 0.1 < ChV < 1 (toxic), and ChV < 0.1 (very toxic).

the appearance of DP9 (formic acid) through pathway-IIB has lowest toxicity, and thus, it shows that the catalytic degradation of CHP by the Bi/Fe^0-5/HSO_5^- system through pathway-IIB is the most suitable and environmentally friendly degradation pathway.

3.6. Hydrogen Production. To achieve the desirable goal of green and clean energy production, the synthesized nano zerovalent iron (Fe^0) and bismuth-doped Fe^0 (Bi/Fe^0-5) were investigated as cheap potential sources of H_2 production from water. Figure 9 depicts H_2 production by Fe^0 and Bi/Fe^0-5. It can be seen that H_2 production could reach to 544 and 712 μM by Fe^0 and Bi/Fe^0-5, respectively, in 70 mL of aqueous solution containing 0.07 g (i.e., at 1 g L^{-1} concentration) of the catalyst at ambient temperature. The theoretical hydrogen yield by Fe^0 could be 1253.58 and 1671.44 μM at 1:1 (shown in reaction 1) and 4:3 (shown in reaction 3) stoichiometry of H_2/Fe^0, respectively. Similarly, the theoretical yield of hydrogen by Bi/Fe^0-5 could be calculated as 1190.90 and 1587.87 μM at 1:1 and 4:3 stoichiometry of H_2/Fe^0, respectively, considering 95% Fe^0 and 5% Bi in Bi/Fe^0-5 and proposing the hydrogen evolution only from Fe^0. In other words, the theoretical yield of hydrogen production from Bi/Fe^0-5 could be 95% of the hydrogen production from Fe^0. Using the above actual and theoretical yields of hydrogen production, one can find the H_2 recovery efficiencies of 43.4 and 32.5% for Fe^0 and 59.8 and 44.8% for Bi/Fe^0-5 at 1:1 (shown in reaction 1) and 4:3 (shown in reaction 3) stoichiometry of H_2/Fe^0, assuming complete dissolution of 1 g L^{-1} Fe^0 (i.e., 0.07 g of Fe^0 and Bi/Fe^0-5 in 70 mL of reaction solution). Because the above data was collected for 72 h of Fe^0 and Bi/Fe^0-5 dissolutions in water, this recovery efficiency can further be increased by allowing more time to Fe^0 and Bi/Fe^0-5 dissolutions. However, the abundant availability of Fe at extremely low cost compared to other H_2-generator catalysts such as noble metals, the obtained H_2 recoveries are still more than sufficient to persuade the green energy production companies and investors to boost up the practical applications of Fe^0 for H_2 production. Interestingly, the doping of a less active metal, that is, a metal with a higher redox potential, at the surface of iron (bimetallic iron system) has been demonstrated to considerably accelerate H_2 production.[25,51,52] That is why Bi/Fe^0-5 showed higher H_2 yield than Fe^0, that is, 712 versus 544 μmol. When attached to a metal having higher redox potential, Fe^0 oxidizes more rapidly and therefore accelerates iron corrosion leading to higher H_2 production. The iron-less active metal couple forms numerous galvanic cells. In such galvanic cells, Fe^0 serves as an anode and readily loses electrons. Meanwhile, the less active metal (i.e., Bi in this case), acting as the cathode, is protected and therefore remains unchanged. The standard redox potentials of Fe/Fe^{2+} and Bi/Bi^{3+} couples relative to the standard hydrogen electrode are −0.44 and +0.308, respectively, suggesting the ability of Fe^0 as the anode and Bi as the cathode when working as galvanic cell electrodes. Besides, the doping of Bi at the surface of Fe^0 reduces the particle size and enhances the BET surface area. For example, in the present study, the particle size and BET surface area for Fe^0 and Bi/Fe^0-5 were calculated to be 16.38 and 6.78 nm and 46.53 and 112.31 m^2 g^{-1}, respectively. Thus, apart from the galvanizing effect produced by Bi in the crystal lattice of Fe^0, the smaller particle and higher surface area of Bi/Fe^0-5 than Fe^0 could possibly be contributed to the relatively higher hydrogen production by Bi/Fe^0-5 as compared to Fe^0 (i.e., 712 vs 544 μmol). The present study underscores the importance of Fe^0, a readily available and inexpensive reductant, for green energy production in addition to its use for water remediation. The ability of less active metals to improve the oxidizing capability of Fe^0 opens new windows and paves the way for the roadmap of Fe^0 research in the fields of water treatments and clean energy productions.

https://dx.doi.org/10.1021/acsomega.0c04574
ACS Omega 2020, 5, 30610−30624

3.7. Environmental Implications. The proposed Bi/Fe^0 system could be not only beneficial as an effective water treatment protocol but also suitable for the production of hydrogen as clean fuel and thus makes it an environmentally benign system. In the present study, the magnetic behavior of the Bi/Fe^0 system and its capability to produce ROS under dark without the need of any electricity/energy source has significantly enhanced its importance for the economical treatment of polluted water or subsurface environments. Furthermore, hydrogen, produced from the Bi/Fe^0/water system, being a clean fuel (without the common impurities such as CO_2 and CH_4) with a high energy to mass ratio, is regarded as a promising candidate compared to alternative energy sources.[23] In this study, the higher hydrogen production by Bi/Fe^0-5 as compared to Fe^0 (i.e., 712 vs 544 μmol) suggests that the hydrogen production rate can be further increased by simply doping Fe^0 with Bi at an appropriate ratio and thus serves as evidence that such technology can be sustainable and economic. The investigated Bi/Fe^0 system operates under ambient temperature and pressure for hydrogen production and thus shows that it could be easily scaled-up for large-scale production.

Although, in the present study, the Bi/Fe^0 system has shown great removal performance, however, in real engineering application, the Bi/Fe^0 system may face a complex environment, and there are numerous conditions that may influence the applicability of the Bi/Fe^0 system in a sustainable treatment process. Therefore, to widely and wisely apply Bi/Fe^0 system in subsurface and water treatment processes, further studies, such as the influence of pollutant concentration, influence of natural organic matter, and degradation in real water and wastewater samples, are underway to reveal the whole picture.

4. CONCLUSIONS

The doping of bismuth into the surface of Fe^0 is an effective way to enhance the reductive capability/activity of Fe^0. The present study reveals that Bi/Fe^0-5/HSO_5^- is an efficient alternative for the treatment of (waste)water containing antibiotics. Interestingly, the Bi/Fe^0-5/HSO_5^- system shows appreciable activity at neutral pH albeit little lower than that at acidic pH. The scavenging experiments illustrate that both $^{\bullet}OH$ and $SO_4^{\bullet-}$ are involved in the degradation of CHP by the Bi/Fe^0-5/HSO_5^- process, although the role of $SO_4^{\bullet-}$ was more predominant. The competition kinetic studies showed that the second-order rate constants of $^{\bullet}OH$ and $SO_4^{\bullet-}$ with CHP are 5.5×10^9 and 3.2×10^9 M^{-1} s^{-1}, respectively. The toxicity assessment of CHP and its DPs showed that the route leading to the formation of formic acid (DP9) (pathway-IIB) is the most suitable and environmentally friendly degradation route. Furthermore, Bi doping at the surface of Fe^0 has beneficial effect on hydrogen production from water decomposition.

■ ASSOCIATED CONTENT

Supporting Information

The Supporting Information is available free of charge at https://pubs.acs.org/doi/10.1021/acsomega.0c04574.

Additional information about the concentration of $SO_4^{\bullet-}$ and $^{\bullet}OH$ in the Bi/Fe^0-5/HSO_5^- system, properties of the DPs, EDX and PL spectra of the nanomaterials, point of zero charge (pH_{PZC}) of Bi/Fe^0-5, % removal of TOC of CHP degradation by Bi/Fe^0-5 and Bi/Fe^0-5/HSO_5^- processes, and cyclic performance of the Bi/Fe^0-5/HSO_5^- process (PDF)

■ AUTHOR INFORMATION

Corresponding Authors

Murtaza Sayed − *Radiation Chemistry Laboratory, National Centre of Excellence in Physical Chemistry, University of Peshawar, Peshawar 25120, Pakistan;* orcid.org/0000-0002-2194-8058; Email: murtazasayed@uop.edu.pk

Noor S. Shah − *Department of Environmental Sciences, COMSATS University Islamabad, Vehari 61100, Pakistan*; Email: noorsamad@ciitvehari.edu.pk

Javed Ali Khan − *Radiation Chemistry Laboratory, National Centre of Excellence in Physical Chemistry, University of Peshawar, Peshawar 25120, Pakistan*; Phone: +92 91 9216766; Email: khanjaved2381@gmail.com; Fax: +92 91 9216671

Authors

Aamir Khan − *Radiation Chemistry Laboratory, National Centre of Excellence in Physical Chemistry, University of Peshawar, Peshawar 25120, Pakistan*

Sajid Rauf − *Hubei Collaborative Innovation Center for Advanced Organic Chemical Materials, Faculty of Physics and Electronic Science, Hubei University, Wuhan, Hubei 430062, PR China*

Faiza Rehman − *Department of Chemistry, University of Poonch, Rawalakot 12350, Azad Kashmir, Pakistan*

Abdullah A. Al-Kahtani − *Chemistry Department, College of Science, King Saud University, Riyadh 11451, Saudi Arabia*

Jibran Iqbal − *College of Natural and Health Sciences, Zayed University, 144534 Abu Dhabi, United Arab Emirates*

Grzegorz Boczkaj − *Department of Process Engineering and Chemical Technology, Faculty of Chemistry, Gdansk University of Technology, Gdansk 80-233, Poland*

Ikhtiar Gul − *Radiation Chemistry Laboratory, National Centre of Excellence in Physical Chemistry, University of Peshawar, Peshawar 25120, Pakistan*

Maleeha Bushra − *Radiation Chemistry Laboratory, National Centre of Excellence in Physical Chemistry, University of Peshawar, Peshawar 25120, Pakistan*

Complete contact information is available at: https://pubs.acs.org/10.1021/acsomega.0c04574

Notes

The authors declare no competing financial interest.

■ ACKNOWLEDGMENTS

The authors would like to acknowledge the financial support and research facilities from National Centre of Excellence in Physical Chemistry, University of Peshawar, Pakistan. F.R. acknowledges support from Higher Education Commission of Pakistan through Startup research grant [SRGP project no. 2033]. N.S.S. acknowledges Higher Education Commission, Pakistan project under the National Research Program for Universities, grant no. 8301/Federal/NRPU/R&D/HEC/2017. J.I. acknowledges the support from Zayed University, Abu Dhabi, UAE under the RIF grant R19052. The authors are also grateful to the Researchers Supporting Project number (RSP-2020/266), King Saud University, Riyadh, Saudi Arabia for the financial support.

REFERENCES

(1) Gul, I.; Sayed, M.; Shah, N. S.; Khan, J. A.; Polychronopoulou, K.; Iqbal, J.; Rehman, F. Solar Light Responsive Bismuth Doped Titania with Ti^{3+} for Efficient Photocatalytic Degradation of Flumequine: Synergistic Role of Peroxymonosulfate. *Chem. Eng. J.* **2020**, *384*, 123255.

(2) Sacco, O.; Vaiano, V.; Rizzo, L.; Sannino, D. Intensification of ceftriaxone degradation under UV and solar light irradiation in presence of phosphors based structured catalyst. *Chem. Eng. Process* **2019**, *137*, 12−21.

(3) Wang, J.; Zhuan, R.; Chu, L. The occurrence, distribution and degradation of antibiotics by ionizing radiation: an overview. *Sci. Total Environ.* **2019**, *646*, 1385−1397.

(4) Chen, X.; Miao, W.; Yang, Y.; Hao, S.; Mao, S. Aeration-assisted sulfite activation with ferrous for enhanced chloramphenicol degradation. *Chemosphere* **2020**, *238*, 124599.

(5) Lin, H.-P.; Chen, C.-C.; Lee, W. W.; Lai, Y.-Y.; Chen, J.-Y.; Chen, Y.-Q.; Fu, J.-Y. Synthesis of a SrFeO3− x/gC3N4 heterojunction with improved visible-light photocatalytic activities in chloramphenicol and crystal violet degradation. *RSC Adv.* **2016**, *6*, 2323−2336.

(6) Yao, B.; Liu, Y.; Zou, D. Removal of chloramphenicol in aqueous solutions by modified humic acid loaded with nanoscale zero-valent iron particles. *Chemosphere* **2019**, *226*, 298−306.

(7) Yu, J.; Hou, X.; Hu, X.; Yuan, H.; Wang, J.; Chen, C. Efficient Degradation of Chloramphenicol by Zero-Valent Iron Microspheres and New Insights in Mechanisms. *Appl. Catal. B* **2019**, *256*, 117876.

(8) Görmez, F.; Görmez, Ö.; Gözmen, B.; Kalderis, D. Degradation of chloramphenicol and metronidazole by electro-Fenton process using graphene oxide-Fe3O4 as heterogeneous catalyst. *J. Environ. Chem. Eng.* **2019**, *7*, 102990.

(9) Anjali, R.; Shanthakumar, S. Insights on the current status of occurrence and removal of antibiotics in wastewater by advanced oxidation processes. *J. Environ. Manage.* **2019**, *246*, 51−62.

(10) Khan, J. A.; Sayed, M.; Khan, S.; Shah, N. S.; Dionysiou, D. D.; Boczkaj, G. Advanced oxidation processes for the treatment of contaminants of emerging concern. *Contaminants of Emerging Concern in Water and Wastewater. Advanced Treatment Processes*; Elsevier, 2019; p 299.

(11) Li, C.; Wu, J.; Peng, W.; Fang, Z.; Liu, J. Peroxymonosulfate activation for efficient sulfamethoxazole degradation by Fe3O4/β-FeOOH nanocomposites: coexistence of radical and non-radical reactions. *Chem. Eng. J.* **2019**, *356*, 904−914.

(12) Bouzayani, B.; Rosales, E.; Pazos, M.; Elaoud, S. C.; Sanromán, M. A. Homogeneous and heterogeneous peroxymonosulfate activation by transition metals for the degradation of industrial leather dye. *J. Cleaner Prod.* **2019**, *228*, 222−230.

(13) Lim, J.; Yang, Y.; Hoffmann, M. R. Activation of Peroxymonosulfate by Oxygen Vacancies-enriched Cobalt-doped Black TiO2 Nanotubes for Removal of Organic Pollutants. *Environ. Sci. Technol.* **2019**, *53*, 6972−6980.

(14) Qi, C.; Liu, X.; Ma, J.; Lin, C.; Li, X.; Zhang, H. Activation of peroxymonosulfate by base: implications for the degradation of organic pollutants. *Chemosphere* **2016**, *151*, 280−288.

(15) Petallidou, K. C.; Polychronopoulou, K.; Boghosian, S.; Garcia-Rodriguez, S.; Efstathiou, A. M. Water−Gas Shift Reaction on Pt/$Ce_{1-x}Ti_xO_{2-\delta}$: The Effect of Ce/Ti Ratio. *J. Phys. Chem. C* **2013**, *117*, 25467−25477.

(16) Charisiou, N. D.; Siakavelas, G.; Tzounis, L.; Sebastian, V.; Monzon, A.; Baker, M. A.; Hinder, S. J.; Polychronopoulou, K.; Yentekakis, I. V.; Goula, M. A. An in depth investigation of deactivation through carbon formation during the biogas dry reforming reaction for Ni supported on modified with CeO_2 and La_2O_3 zirconia catalysts. *Int. J. Hydrogen Energy* **2018**, *43*, 18955−18976.

(17) Shah, N. S.; Khan, J. A.; Sayed, M.; Khan, Z. U. H.; Iqbal, J.; Imran, M.; Murtaza, B.; Zakir, A.; Polychronopoulou, K. Nano zerovalent zinc catalyzed peroxymonosulfate based advanced oxidation technologies for treatment of chlorpyrifos in aqueous solution: A semi-pilot scale study. *J. Cleaner Prod.* **2020**, *246*, 119032.

(18) Iqbal, J.; Shah, N. S.; Sayed, M.; Imran, M.; Muhammad, N.; Howari, F. M.; Alkhoori, S. A.; Khan, J. A.; Haq Khan, Z. U.; Bhatnagar, A.; Polychronopoulou, K.; Ismail, I.; Haija, M. A. Synergistic effects of activated carbon and nano-zerovalent copper on the performance of hydroxyapatite-alginate beads for the removal of As3+ from aqueous solution. *J. Cleaner Prod.* **2019**, *235*, 875−886.

(19) Murtaza, B.; Shah, N. S.; Sayed, M.; Khan, J. A.; Imran, M.; Shahid, M.; Khan, Z. U. H.; Ghani, A.; Murtaza, G.; Muhammad, N.; Khalid, M. S.; Niazi, N. K. Synergistic effects of bismuth coupling on the reactivity and reusability of zerovalent iron nanoparticles for the removal of cadmium from aqueous solution. *Sci. Total Environ.* **2019**, *669*, 333−341.

(20) Qiu, X.; Fang, Z.; Liang, B.; Gu, F.; Xu, Z. Degradation of decabromodiphenyl ether by nano zero-valent iron immobilized in mesoporous silica microspheres. *J. Hazard. Mater.* **2011**, *193*, 70−81.

(21) Suanon, F.; Sun, Q.; Li, M.; Cai, X.; Zhang, Y.; Yan, Y.; Yu, C.-P. Application of nanoscale zero valent iron and iron powder during sludge anaerobic digestion: Impact on methane yield and pharmaceutical and personal care products degradation. *J. Hazard. Mater.* **2017**, *321*, 47−53.

(22) Raman, C. D.; Kanmani, S. Textile dye degradation using nano zero valent iron: a review. *J. Environ. Manage.* **2016**, *177*, 341−355.

(23) Qin, H.; Guan, X.; Bandstra, J. Z.; Johnson, R. L.; Tratnyek, P. G. Modeling the kinetics of hydrogen formation by zerovalent iron: Effects of sulfidation on micro-and nano-scale particles. *Environ. Sci. Technol.* **2018**, *52*, 13887−13896.

(24) Reardon, E. J. Zerovalent irons: Styles of corrosion and inorganic control on hydrogen pressure buildup. *Environ. Sci. Technol.* **2005**, *39*, 7311−7317.

(25) Chen, K.-F.; Li, S.; Zhang, W.-x. Renewable hydrogen generation by bimetallic zero valent iron nanoparticles. *Chem. Eng. J.* **2011**, *170*, 562−567.

(26) Schikorr, G. Über die Reaktionen zwischen Eisen, Seinen Hydroxyden und Wasser. *Z. Angew. Phys.* **1929**, *35*, 65−70.

(27) Shipko, F. J.; Douglas, D. L. Stability of ferrous hydroxide precipitates. *J. Phy. Chem.* **1956**, *60*, 1519−1523.

(28) Odziemkowski, M. S.; Schuhmacher, T. T.; Gillham, R. W.; Reardon, E. J. Mechanism of oxide film formation on iron in simulating groundwater solutions: Raman spectroscopic studies. *Corros. Sci.* **1998**, *40*, 371−389.

(29) Li, Z.; Sun, Y.; Yang, Y.; Han, Y.; Wang, T.; Chen, J.; Tsang, D. C. W. Biochar-supported nanoscale zero-valent iron as an efficient catalyst for organic degradation in groundwater. *J. Hazard. Mater.* **2020**, *383*, 121240.

(30) Gong, J.; Lee, C.-S.; Chang, Y.-Y.; Chang, Y.-S. Novel self-assembled bimetallic structure of Bi/Fe^0: The oxidative and reductive degradation of hexahydro-1,3,5-trinitro-1,3,5-triazine (RDX). *J. Hazard. Mater.* **2015**, *286*, 107−117.

(31) Marková, Z.; Šišková, K. M.; Filip, J.; Čuda, J.; Kolář, M.; Šafářová, K.; Medřík, I.; Zbořil, R. Air stable magnetic bimetallic Fe−Ag nanoparticles for advanced antimicrobial treatment and phosphorus removal. *Environ. Sci. Technol.* **2013**, *47*, 5285−5293.

(32) Rastogi, A.; Al-Abed, S. R.; Dionysiou, D. D. Sulfate radical-based ferrous−peroxymonosulfate oxidative system for PCBs degradation in aqueous and sediment systems. *Appl. Catal. B* **2009**, *85*, 171−179.

(33) Cheng, X.; Liang, H.; Ding, A.; Tang, X.; Liu, B.; Zhu, X.; Gan, Z.; Wu, D.; Li, G. Ferrous iron/peroxymonosulfate oxidation as a pretreatment for ceramic ultrafiltration membrane: Control of natural organic matter fouling and degradation of atrazine. *Water Res.* **2017**, *113*, 32−41.

(34) Barzegar, G.; Jorfi, S.; Zarezade, V.; Khatebasreh, M.; Mehdipour, F.; Ghanbari, F. 4-Chlorophenol degradation using ultrasound/peroxymonosulfate/nanoscale zero valent iron: reusability, identification of degradation intermediates and potential application for real wastewater. *Chemosphere* **2018**, *201*, 370−379.

https://dx.doi.org/10.1021/acsomega.0c04574
ACS Omega 2020, 5, 30610−30624

(35) Oh, W.-D.; Dong, Z.; Ronn, G.; Lim, T.-T. Surface−active bismuth ferrite as superior peroxymonosulfate activator for aqueous sulfamethoxazole removal: performance, mechanism and quantification of sulfate radical. *J. Hazard. Mater.* **2017**, *325*, 71−81.
(36) Joo, S. H.; Feitz, A. J.; Sedlak, D. L.; Waite, T. D. Quantification of the oxidizing capacity of nanoparticulate zero-valent iron. *Environ. Sci. Technol.* **2005**, *39*, 1263−1268.
(37) Li, X.; Liu, X.; Lin, C.; Zhou, Z.; He, M.; Ouyang, W. Catalytic oxidation of contaminants by Fe0 activated peroxymonosulfate process: Fe (IV) involvement, degradation intermediates and toxicity evaluation. *Chem. Eng. J.* **2020**, *382*, 123013.
(38) Lindsey, M. E.; Tarr, M. A. Quantitation of hydroxyl radical during Fenton oxidation following a single addition of iron and peroxide. *Chemosphere* **2000**, *41*, 409−417.
(39) Huang, T.; Zhang, G.; Zhang, N.; Ye, J.; Lu, P. Fe0-H_2O_2 for advanced treatment of citric acid wastewater: Detailed study of catalyst after several times use. *Chem. Eng. J.* **2018**, *336*, 233−240.
(40) Zhang, X.; Lin, S.; Chen, Z.; Megharaj, M.; Naidu, R. Kaolinite-supported nanoscale zero-valent iron for removal of Pb2+ from aqueous solution: reactivity. characterization and mechanism. *Water Res.* **2011**, *45*, 3481−3488.
(41) Holzwarth, U.; Gibson, N. The Scherrer equation versus the "Debye-Scherrer equation". *Nat. Nanotechnol.* **2011**, *6*, 534.
(42) Li, X.-q.; Zhang, W.-x. Sequestration of metal cations with zerovalent iron nanoparticles a study with high resolution X-ray photoelectron spectroscopy (HR-XPS). *J. Phys. Chem. C* **2007**, *111*, 6939−6946.
(43) Woo, H.; Park, J.; Lee, S.; Lee, S. Effects of washing solution and drying condition on reactivity of nano-scale zero valent irons (nZVIs) synthesized by borohydride reduction. *Chemosphere* **2014**, *97*, 146−152.
(44) Cao, J.; Lai, L.; Lai, B.; Yao, G.; Chen, X.; Song, L. Degradation of tetracycline by peroxymonosulfate activated with zero-valent iron: Performance, intermediates, toxicity and mechanism. *Chem. Eng. J.* **2019**, *364*, 45−56.
(45) Wang, Z.; Qiu, W.; Pang, S.; Gao, Y.; Zhou, Y.; Cao, Y.; Jiang, J. Relative contribution of ferryl ion species (Fe(IV)) and sulfate radical formed in nanoscale zero valent iron activated peroxydisulfate and peroxymonosulfate processes. *Water Res.* **2020**, *172*, 115504.
(46) Buxton, G. V.; Greenstock, C. L.; Helman, W. P.; Ross, A. B. Critical review of rate constants for reactions of hydrated electrons, hydrogen atoms and hydroxyl radicals ($^{\bullet}OH/^{\bullet}O^{-}$) in aqueous solution. *J. Phys. Chem. Ref. Data* **1988**, *17*, 513−886.
(47) Neta, P.; Madhavan, V.; Zemel, H.; Fessenden, R. W. Rate constants and mechanism of reaction of sulfate radical anion with aromatic compounds. *J. Am. Chem. Soc.* **1977**, *99*, 163−164.
(48) Tan, C.; Dong, Y.; Fu, D.; Gao, N.; Ma, J.; Liu, X. Chloramphenicol removal by zero valent iron activated peroxymonosulfate system: Kinetics and mechanism of radical generation. *Chem. Eng. J.* **2018**, *334*, 1006−1015.
(49) Li, W.; Zhou, J. Z.; Zhang, J.; Zhao, J.; Xu, Y.; Qian, G. pH-Dependent improvement of pyrophosphate removal on amorphous ferric hydroxide by incorporating Ca^{2+}. *Chem. Eng. J.* **2013**, *225*, 372−377.
(50) Chen, J.; Xia, Y.; Dai, Q. Electrochemical degradation of chloramphenicol with a novel Al doped PbO_2 electrode: Performance, kinetics and degradation mechanism. *Electrochim. Acta* **2015**, *165*, 277−287.
(51) Zhang, W.-x.; Wang, C.-B.; Lien, H.-L. Treatment of chlorinated organic contaminants with nanoscale bimetallic particles. *Catal. Today* **1998**, *40*, 387−395.
(52) Zhu, B.-W.; Lim, T.-T. Catalytic reduction of chlorobenzenes with Pd/Fe nanoparticles: reactive sites, catalyst stability, particle aging, and regeneration. *Environ. Sci. Technol.* **2007**, *41*, 7523−7529.

https://dx.doi.org/10.1021/acsomega.0c04574
ACS Omega 2020, 5, 30610−30624